1521-0111/88/5/926–934$25.00
MOLECULAR PHARMACOLOGY

http://dx.doi.org/10.1124/mol.115.100107
Mol Pharmacol 88:926–934, November 2015

Breathing Stimulant Compounds Inhibit TASK-3 Potassium Channel Function Likely by Binding at a Common Site in the Channel Pore[S]

Rikki H. Chokshi, Aaron T. Larsen, Brijesh Bhayana, and Joseph F. Cotten

Department of Anesthesia, Critical Care, and Pain Medicine (R.H.C., J.F.C.), Center for Computational and Integrative Biology, and Department of Molecular Biology (A.T.L.), and Department of Dermatology (B.B.), Massachusetts General Hospital, Boston, Massachusetts

Received May 28, 2015; accepted August 11, 2015

ABSTRACT

Compounds PKTHPP (1-{1-[6-(biphenyl-4-ylcarbonyl)-5,6,7,8-tetrahydropyrido[4,3-d]-pyrimidin-4-yl]piperidin-4-yl}propan-1-one), A1899 (2′′-[(4-methoxybenzoylamino)methyl]biphenyl-2-carboxylic acid 2,4-difluorobenzylamide), and doxapram inhibit TASK-1 (KCNK3) and TASK-3 (KCNK9) tandem pore (K_{2P}) potassium channel function and stimulate breathing. To better understand the molecular mechanism(s) of action of these drugs, we undertook studies to identify amino acid residues in the TASK-3 protein that mediate this inhibition. Guided by homology modeling and molecular docking, we hypothesized that PKTHPP and A1899 bind in the TASK-3 intracellular pore. To test our hypothesis, we mutated each residue in or near the predicted PKTHPP and A1899 binding site (residues 118–128 and 228–248), individually, to a negatively charged aspartate. We quantified each mutation's effect on TASK-3 potassium channel concentration response to PKTHPP. Studies were conducted on TASK-3 transiently expressed in Fischer rat thyroid epithelial monolayers; channel function was measured in an Ussing chamber. TASK-3 pore mutations at residues 122 (L122D, E, or K) and 236 (G236D) caused the IC_{50} of PKTHPP to increase more than 1000-fold. TASK-3 mutants L122D, G236D, L239D, and V242D were resistant to block by PKTHPP, A1899, and doxapram. Our data are consistent with a model in which breathing stimulant compounds PKTHPP, A1899, and doxapram inhibit TASK-3 function by binding at a common site within the channel intracellular pore region, although binding outside the channel pore cannot yet be excluded.

Introduction

TASK-1 (KCNK3) and TASK-3 (KCNK9) proteins are members of the tandem pore (K_{2p}) potassium channel family. There are 15 human tandem pore potassium channels, which in general provide a background "leak" potassium conductance important in determining a cell's resting membrane potential and excitability (Yost, 2003). TASK-1 and TASK-3 proteins share approximately 60% amino acid identity, with similarity highest in their potassium-conducting, pore-forming, membrane-associated domain. TASK potassium channel conductance is inhibited by extracellular acidic pH and is a homo- or heterodimeric channel composed of two TASK-1 protein subunits, two TASK-3 subunits, or one TASK-1 and one TASK-3 subunit. Crystal structures of three homologous members of the human family, TWIK-1, TRAAK, and TREK-2, were recently solved (Brohawn et al., 2012; Miller and Long, 2012; Lolicato et al., 2014; Dong et al., 2015). These structures have markedly advanced understanding of tandem pore structure and function and support homology model development to guide TASK studies (Fig. 1).

TASK-1 and TASK-3 channels are widely expressed in various tissues, including the cerebral cortex (Callahan et al., 2004), the brainstem pre-Botzinger and retrotrapezoid regions (Mulkey et al., 2007; Koizumi et al., 2010), the carotid bodies (Buckler et al., 2000), hypoglossal and spinal cord motor neurons (Lazarenko et al., 2010), pulmonary artery smooth muscle (Olschewski et al., 2006), the adrenal cortex (Czirjak and Enyedi, 2002), and the atrium of the heart (Limberg et al., 2011). The TASK-3 channel is also overexpressed in a variety of cancers and confers hypoxia resistance on tumors (Mu et al., 2003). Knockout mice lacking one or both TASK channels display a variety of phenotypes, including impaired carotid body chemosensing (Ortega-Saenz et al., 2010), sleep fragmentation (Pang et al., 2009), antidepressive behavior (Gotter et al., 2011), primary hyperaldosteronism and low-renin essential hypertension (Davies et al., 2008; Guagliardo et al., 2012), and cardiac conduction and repolarization abnormalities (Decher et al., 2011; Donner et al., 2011;

This research was supported by the Massachusetts General Hospital Department of Anesthesia, Critical Care and Pain Medicine; the National Institutes of Health [Grant HL117871]; the Simons Collaboration on the Origins of Life; the Fonds de recherche du Québec, Nature et technologies; and the Autonomous Province of Trento.
dx.doi.org/10.1124/mol.115.100107.
[S] This article has supplemental material available at molpharm.aspetjournals.org.

ABBREVIATIONS: A1899, 2′′-[(4-methoxybenzoylamino)methyl]biphenyl-2-carboxylic acid 2,4-difluorobenzylamide; AVE0118, N-(2-pyridin-3-ylethyl)-2′-{[2-(4-methoxyphenyl)acetylamino]-methyl}biphenyl-2-carboxamide; DMSO, dimethylsulfoxide; NEM, *N*-ethylmaleimide; PKTHPP, 1-{1-[6-(biphenyl-4-ylcarbonyl)-5,6,7,8-tetrahydropyrido[4,3-d]-pyrimidin-4-yl]piperidin-4-yl}propan-1-one.

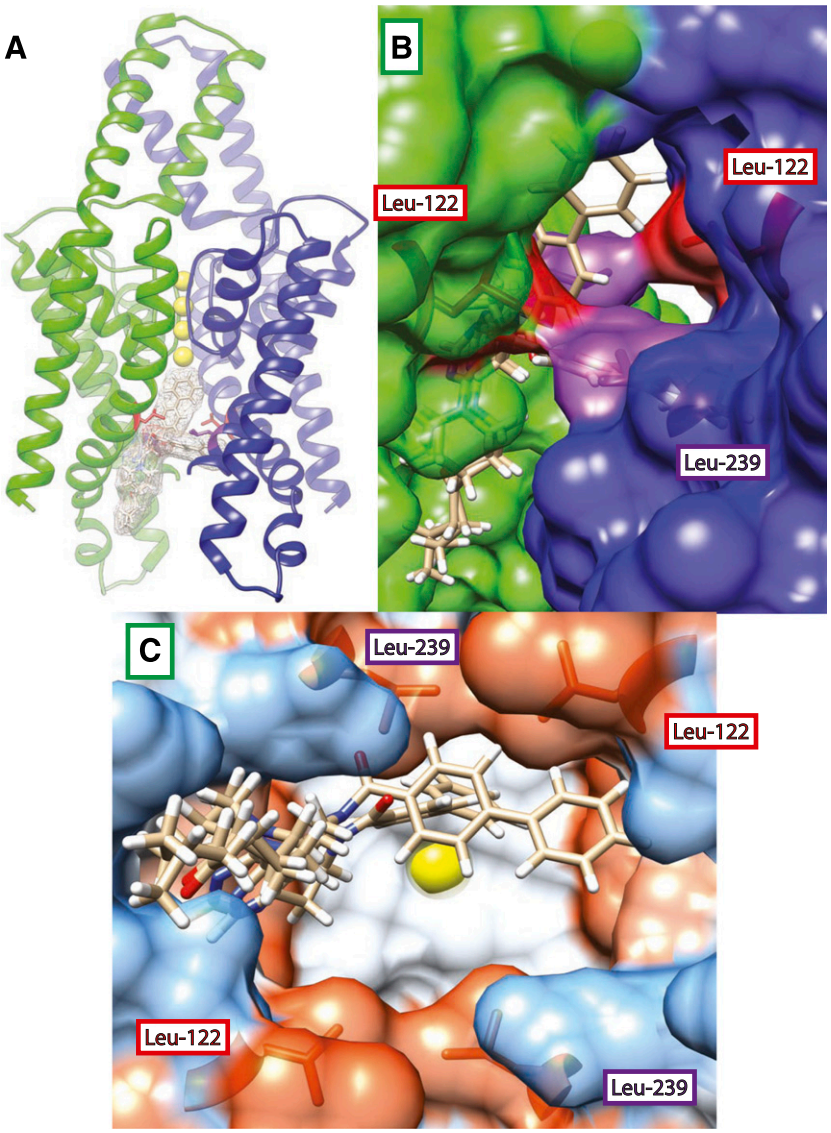

Fig. 1. (A) Homology model of TASK-3 potassium channel and docking predictions for PKTHPP. Top two poses for PKTHPP are superimposed within the TASK-3 pore. Residues Leu-122 (colored red) and Leu-239 (colored purple) are shown within TASK-3 subunit A (colored green) and subunit B (colored blue). (B) Side/membrane view through fenestration into pore; note close proximity of Leu-122 (colored red) and Leu-239 (colored purple). (C) Bottom/cytoplasmic view "looking up" into pore. Molecular surfaces are colored by Kyte-Doolittle amino acid hydrophobicity (dodger blue for the most hydrophilic, to white, to orange-red for most hydrophobic). Potassium ions (colored yellow) are present in the pore selectivity filter of each image.

Petric et al., 2012). An inactivating mutation in the human TASK-3 channel pore (G236R) is associated with the Birk-Barel syndrome of mental retardation, hypotonia, and facial dysmorphism (Barel et al., 2008). Inactivating mutations in human TASK-1 (G203D, G97R, V221L, E182K, T8K, Y192C) are associated with familial pulmonary arterial hypertension (Ma et al., 2013) and atrial arrhythmias (V123L) (Liang et al., 2014).

Drugs that modulate TASK function may have utility in the treatment of breathing disorders such as sleep apnea or drug-induced ventilatory depression, cardiac atrial dysrhythmias, sleep disorders, neurodegenerative disorders, major depression, and/or malignancy. A number of selective, high-potency TASK-blocking compounds have been identified, and some are in clinical use or have undergone preclinical studies (Putzke et al., 2007; Brendel et al., 2009; Streit et al., 2011; Coburn et al., 2012; Flaherty et al., 2014). Doxapram is a breathing stimulant and carotid body–activating drug developed in the 1960s for use in human and veterinary medicine (Lunsford et al., 1964). Doxapram may act on TASK-1/TASK-3 heterodimeric channels, which provide the predominant hypoxia-sensitive background potassium conductance in rodent carotid body glomus cells (Cotten et al., 2006; Kim et al., 2009). Other potent TASK blockers, including PKTHPP (Compound 23; Merck, Kenilworth, New Jersey), A1899 (S20951; Sanofi Aventis, Paris, France), AVE0118 [N-(2-pyridin-3-ylethyl)-2′-{[2-(4-methoxyphenyl) acetylamino]-methyl}biphenyl-2-carboxamide (Sanofi Aventis)], and related analogs, cause stimulation of breathing in rats (Brendel et al., 2009; Cotten, 2013) and rabbits (Brendel et al., 2009) and promote airway patency in rat (Brendel et al., 2009) and pig models (Wirth et al., 2013; Kiper et al., 2015) of obstructive sleep apnea. TASK-1 expression in human and pig hearts, unlike that in rodents, is limited to the atria and promotes action potential recovery (Limberg et al., 2011; Schmidt et al., 2014). TASK-1–inhibiting compounds increase cardiac atrial tissue refractoriness and may prevent and/or treat atrial fibrillation (Wirth et al., 2003, 2007; Kiper et al., 2015). Other TASK-inhibiting drugs with known cardiac pro- or antiarrhythmic properties include lidocaine, bupivacaine, amiodarone, and carvedilol (Kindler et al., 1999; Gierten et al., 2010; Staudacher et al., 2011).

Mutagenesis and modeling studies of TASK-1 by Streit et al. (2011) and Kiper et al. (2015) using A1899 and other inhibitory compounds have suggested an intracellular potassium channel pore site of action. We undertook homology modeling, docking, and scanning aspartate mutagenesis studies to determine where on the TASK-3 channel the breathing stimulant compounds PKTHPP, A1899, and doxapram act. Our results are consistent with a common site of action on TASK-3, the intracellular pore.

Materials and Methods

Homology Modeling. The sequence of human TASK-3 was downloaded from the universal protein resource (UniProt entry Q9NPC2), and homology modeling was performed using SWISS-MODEL (http://swissmodel.expasy.org/). Models were generated based upon two structural templates, PDB 3UM7 (TRAAK) and PDB 3UKM (TWIK-1), which share high sequence identity with TASK-3 (35.19 and 30.54%, respectively). Both templates here are K+ ion channels, affording high confidence that they share structural similarities with the target protein. The model generated using the 3UKM (TWIK-1) template was preferred based upon its superior QMEAN score (Benkert et al., 2009) and the significant amount of random coil in the TRAAK-based model. The TWIK-1–based homology model was superimposed on PDB 3UKM using the Discovery Studio 3.5 Visualizer (BIOVIA, San Diego, CA) before molecular docking.

Molecular Docking. Docking studies were performed using the Molecular Forecaster suite of docking software developed at and licensed by McGill University (Montreal, QC, Canada) (Moitessier et al., 2004) and its associated modules. Default settings were used unless otherwise noted. The protein structure of TASK-3 generated by homology modeling was prepared using the PROCESS module with a ligand cutoff of 60 Å. Ligands to be docked were prepared using the SMART module. Docking calculations using the entire TASK-3 protein were performed using the FITTED module with the "rigid" protein setting. The final top-scoring (i.e., lowest energy) binding poses/locations were considered as reasonable initial guesses for protein/ligand interaction sites.

Molecular Biology. Rat TASK-3 was cloned into variants of the pcDNA3.1 vector (Invitrogen, Carlsbad, CA). Mutations were introduced into cDNAs by high-fidelity polymerase chain reaction with a Q5 Mutagenesis Kit (New England BioLabs, Ipswich, MA) or using the method of overlapping extension (Phusion HF Mastermix; New England BioLabs). The sequence of all mutant cDNA was confirmed through bidirectional sequencing (Massachusetts General Hospital DNA Core Facility, Cambridge, MA).

The TASK-3 dimers were prepared by ligating a polymerase chain reaction fragment encoding wild-type or L122D TASK-3 cDNA, minus its stop codon, between restriction sites HindIII and KpnI upstream of L122D or wild-type TASK-3 coding sequence in the pcDNA3.1/V5-His-TOPO-TA vector (Invitrogen). This introduced an 18–amino acid linker sequence (LVPSSDPLVQCGGIALAT) between TASK-3 subunits.

Cell Culture, Transfection, and Ussing Chamber Studies. Fischer rat thyroid epithelial cells were maintained in Ham's F-12 medium supplemented with 5% fetal calf serum (Sigma-Aldrich, St. Louis, MO) at 37°C and 5% CO_2 in a humidified incubator. Following trypsinization, cells were pipetted onto semipermeable supports (~1.5×10^5 cells per support; Corning Snapwell polycarbonate; 0.4-μm pore size, 12-mm diameter; Fisher Scientific, Pittsburgh, PA) and transfected while still in suspension using Lipofectamine 2000 (Invitrogen). Transfected monolayers were studied 48 hours after transfection in a custom-built Ussing chamber.

Ussing chamber methods were based on that described in Sheppard et al. (1994). Junction potentials were offset prior to placement of a study monolayer in the chamber. A potassium gradient was applied across each study monolayer, and the transepithelial voltage was clamped at 0 mV (DVC-1000 amplifier; World Precision Instruments, Sarasota, FL). The potassium concentration gradient provides the only driving force for potassium flux (>100 mV by Nernst equation). Apical bathing solution was as follows (in mM): 135 NaCl, 1.2 $MgCl_2$, 1.2 $CaCl_2$, 10 HEPES, and 10 dextrose (pH 7.4) with NaOH. Basolateral bathing solution was as follows (in mM): 135 KCl, 1.2 $MgCl_2$, 1.2 $CaCl_2$, 10 HEPES, and 10 dextrose (pH 7.4) with KOH. MES was used in lieu of HEPES in the pH 5.5 apical solution. The amplified current signal was digitized with no filtering at 10 Hz using a USB-6009 data acquisition board (National Instruments, Austin, TX) interfaced with an Apple Computer running Labview 8.5 software (National Instruments). Potassium current data were averaged every 1 second for analysis. By convention, positive current indicates positive charge flowing in the basolateral to apical direction. Transepithelial voltage pulses of +5 mV (1-second duration), referenced to the apical surface, were applied intermittently to assess transepithelial resistance and monolayer integrity. Air was continuously bubbled through apical and basolateral solutions. All studies were conducted at room temperature (22–24°C).

Graphing and Statistical Analysis. Data analysis, graphing, and regression were done using Microsoft Excel (Microsoft, Redmond, WA) and Prism 5.0 (GraphPad Software, La Jolla, CA). A one-way analysis of variance and a post-hoc Tukey's multiple comparison test were used to compare group means. For fitted data, an extra sum-of-squares F test in Prism 5.0 was used to individually compare each log IC_{50} determined by nonlinear regression between wild-type TASK-3 and each mutant. The calculated P value for each mutant was multiplied by a Bonferroni correction factor to account for multiple comparisons. Molecular volume and calculated log P were estimated using the Molinspiration online web tool (www.molinspiration.com). Molecular graphics and analyses were performed with the UCSF Chimera package. Chimera is developed by the Resource for Biocomputing, Visualization, and Informatics at the University of California, San Francisco (supported by National Institute of General Medical Sciences P41-GM103311) (Pettersen et al., 2004).

Reagents. PKTHPP and A1899 were custom synthesized by Aberjona Laboratories (Beverly, MA) and Dr. Brijesh Bhayana (Massachusetts General Hospital Department of Dermatology), respectively, using published methods (Peukert et al., 2003; Coburn et al., 2012). PKTHPP and A1899 were solubilized in dimethylsulfoxide (DMSO; 10 mM stock); *N*-ethylmaleimide (NEM) was solubilized in DMSO (1 M stock). From prior work, we know TASK-3 function is unaffected by DMSO at bath concentrations up to 1%, and our concentration-response studies remained below this level. Dopram (doxapram-HCL, 20 mg/ml) was obtained from McKesson Medical-Surgical (Richmond, VA). All other chemical supplies and reagents were obtained from Sigma-Aldrich or Fisher Scientific unless otherwise noted.

Results

TASK-3 Homology Model and PKTHPP and A1899 Docking. Figure 1 shows the superimposition of the best two poses of PKTHPP docked in the TASK-3 homology model pore. PKTHPP binds asymmetrically along one wall of the pore (Fig. 1). In one pose, the biphenyl group extends deep into the pore pointing toward the potassium ions; in the other, the biphenyl folds and crosses the pore. Relative to PKTHPP, A1899 docked deeper in and across the pore with its difluorophenyl group in close proximity to several aliphatic residues (Supplemental Fig. 1). Doxapram, which has an IC_{50} significantly higher than that of PKTHPP and A1899, failed to dock in this model. The TASK-3 model retains the fenestrations observed in TWIK-1 (Miller and Long, 2012). Leu-122 and Leu-239, which are in close approximation, line the aperture of the fenestration (Fig. 1B). Leu-122 and Leu-239

contribute to the overall hydrophobicity of the deep inner TASK-3 pore and a hydrophobic narrowing in the pore diameter (Fig. 1C).

Aspartate Scanning Mutagenesis in the TASK-3 Pore Disrupts PKTHPP Inhibition. The docking studies suggested pore-lining residues in M2 and M4 transmembrane domains contribute to PKTHPP binding (Fig. 1). To test this model, residues in or near the predicted PKTHPP binding site were mutagenized to potentially alter PKTHPP binding. Because PKTHPP is hydrophobic (cLogP = 4.2; Fig. 2A), a polar aspartate residue was introduced, sequentially, at positions 118–128 in the M2 domain of TASK-3 or at residues 228–248 in the M4 domain (Fig. 2B). The PKTHPP concentration response of wild-type TASK-3 and each mutant was determined by Ussing chamber (Fig. 3). Eight of the 33 aspartate mutants failed to provide sufficient current for IC_{50} determination (Fig. 3, E and F; Supplemental Fig. 2). However, of the 25 mutants with sufficient function, 10 demonstrated a greater than 10-fold shift in their PKTHPP IC_{50} relative to wild-type TASK-3 [10 nM; 9–11 (95% confidence), n = 6]. Several TASK-3 mutants had marked (~90- to >1000-fold) increases in their IC_{50}: L122D (>10 μM), G236D (7 μM), L239D (895 nM), and V242D (1.6 μM) (Fig. 3, E and F). PKTHPP solubility limited concentration-response analysis for TASK-3 L122D, and the obtained data could not be fitted with confidence. All of the functional mutants were inhibited by extracellular acidic pH 5.5 (Figs. 3–5 and data not shown).

Residue 122 Amino Acid Requirements for PKTHPP Inhibition. A range of amino acid substitutions were introduced at residue 122 to better understand the requirements on this site for PKTHPP inhibition of TASK-3 function. Similar to that observed with the TASK-3 L122D mutant, other charged residues, both negative (E) or positive (K), had strong effects on PKTHPP IC_{50}, all increasing it greater than ~1000-fold (Fig. 4). However, every substitution at residue 122, polar or hydrophobic, small or large, impaired PKTHPP inhibition to some extent relative to wild-type TASK-3; even the conservative L122I mutation right-shifted PKTHPP IC_{50} ~30-fold (to 310 nM).

A Single-Pore Asp-122 Is Sufficient to Impair PKTHPP Inhibition. The TASK-3 channel is composed of two protein subunits, each contributing one residue 122 to the pore. The subunit composition of TASK-3 channels can be forced by expressing both subunits as a single polypeptide joined by a linker region (Fig. 5A). To determine the number of

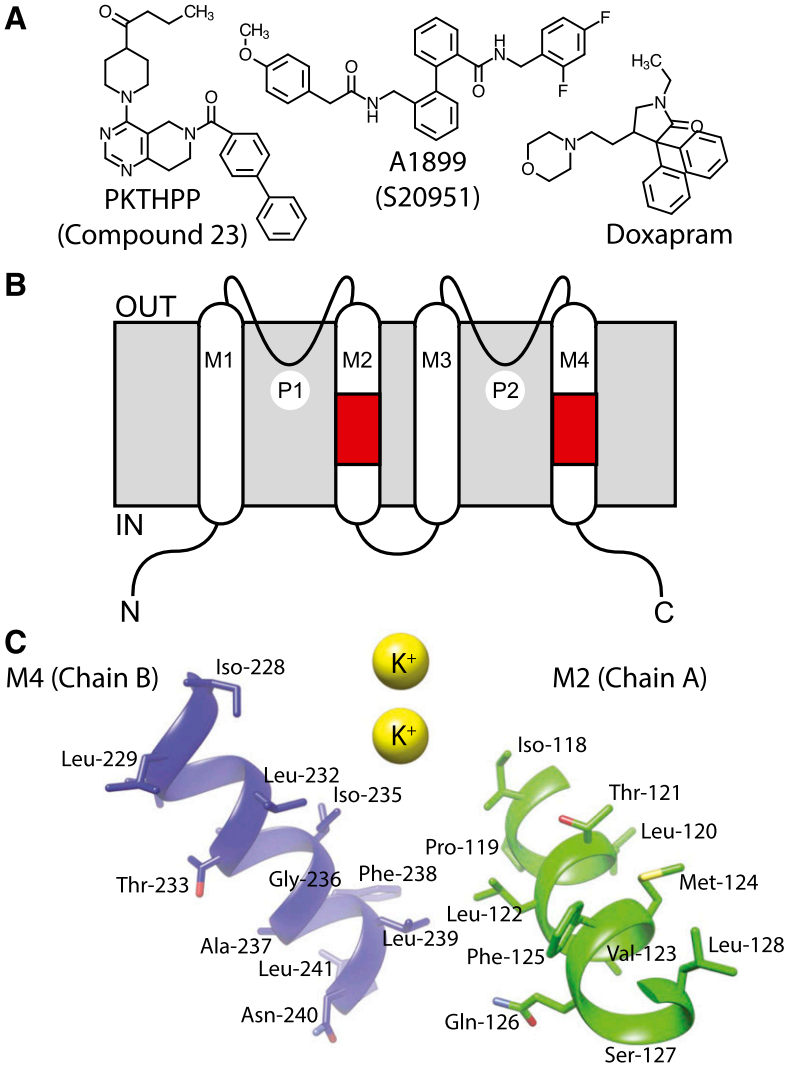

Fig. 2. (A) Chemical structures of PKTHPP, A1899, and doxapram. (B) Illustration of TASK-3 topology and relationship of various domains in primary amino acid structure. Alternate names for PKTHPP (Compound 23) and A1899 (S20951) are in parentheses. Regions of scanning aspartate mutagenesis are colored red (residues 118–128 in M2 and residues 228–241 in M4). (C) Relative orientations of the mutated residues in M2 and M4 to each other and to the pore. IN, intracellular surface; M1–M4, transmembrane domains 1–4; OUT, extracellular surface; P1 and P2, potassium ion selectivity filters 1 and 2.

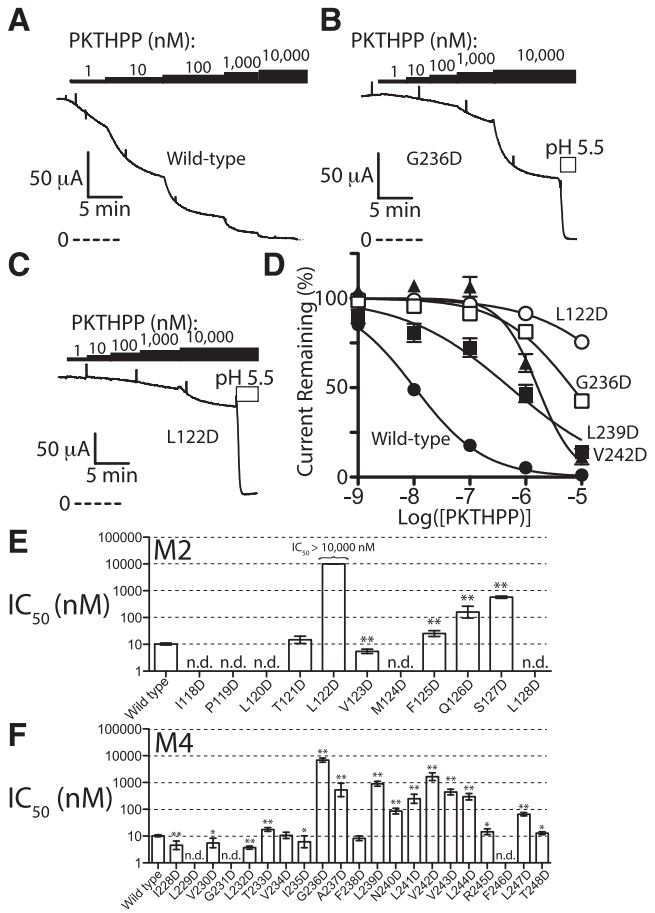

Fig. 3. Scanning aspartate mutagenesis in the inner TASK-3 pore disrupts PKTHPP inhibition. (A–C) Ussing chamber potassium current records using Fischer rat thyroid cell monolayers transiently expressing TASK-3 channels (wild type, G236D, and L122D). Black bars indicate PKTHPP application. Perforated lines indicate zero current level. L-shaped bar indicates current and time scale. (D) Ussing chamber concentration response for PKTHPP; each data point is the mean ± S.E.M. of at least three monolayers. (E and F) Concentration required for 50% inhibition TASK-3 potassium current (IC_{50}). M2 and M4, second and fourth transmembrane domain of TASK-3 protein. IC_{50} results are the mean ± 95% confidence interval from curve fitting of data derived from at least three monolayers each using the following equation: normalized response = 100/(1 + 10^((log[IC_{50}] − log[PKTHPP])*HillSlope)). $^{***}P < 0.001$, $^{**}P < 0.01$, and $^{*}P < 0.05$ relative to wild-type TASK-3. n.d., not determined due to insufficient potassium current.

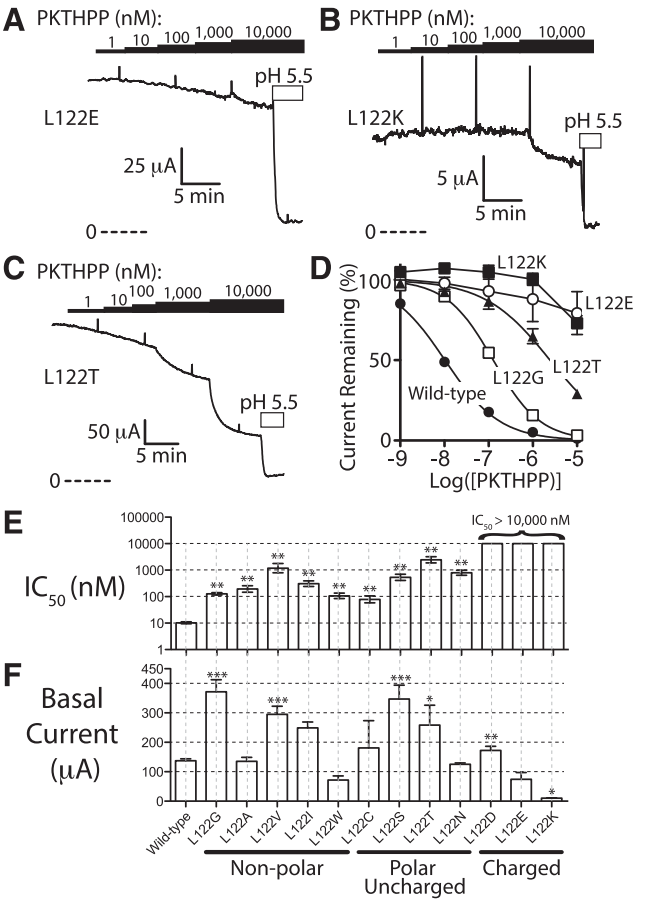

Fig. 4. Most mutations at residue 122 disrupt PKTHPP inhibition, and charged residues are the most disruptive. (A–C) Ussing chamber potassium current records using Fischer rat thyroid cell monolayers transiently expressing rat TASK-3 channels (L122E, L122K, L122T). (D) Ussing chamber concentration response for PKTHPP. (E) Concentration required for 50% inhibition of potassium current (IC_{50}; mean ± 95% confidence; data fitted as in Fig. 3). (F) Basal current levels for each mutant (mean ± S.E.M.; n = at least 3 each). $^{***}P < 0.001$, $^{**}P < 0.01$, and $^{*}P < 0.05$ relative to wild-type TASK-3.

Asp-122 residues required to impair PKTHPP binding, TASK-3 dimeric channels containing two Asp-122s (L122D/L122D), two Leu-122s (wild type/wild type), or one Asp-122 and one Leu-122 (L122D/wild type and wild type/L122D) were prepared and studied. The IC_{50} for PKTHPP inhibition of the wild-type and L122D/L122D TASK-3 homodimers was similar to that of freely associated wild-type and L122D subunits: 5 nM (4–6, $n = 4$) and >10 μM ($n = 4$), respectively (Fig. 5, B and C). The L122D/wild-type and wild-type/L122D heterodimers had PKTHPP sensitivities intermediate to the others, such that a single aspartate in the pore right shifts the PKTHPP IC_{50} ~100-fold to 576 nM (431–770) and 695 nM (492–981, $n = 3$–4), respectively (Fig. 5C).

Aspartate Mutations at Residues 122, 236, 239, and 242 in TASK-3 Impair Inhibition by A1899 and Doxapram. Prior studies have determined that A1899 binds in the TASK-1 pore, and the TASK-1 pore shares significant amino acid homology with that of TASK-3. Additionally, our docking studies suggest A1899 binds in the TASK-3 pore (Supplemental Fig. 1). Consistent with these observations, L122D, G236D, L239D, and V242D mutations all impaired A1899 inhibition of TASK-3 channel function (Fig. 6, A and B). Similar to PKTHPP and A1899, doxapram inhibition of TASK-3 was impaired by the aforementioned mutations as well, although to a lesser extent (Fig. 6, C and D).

Gating Mutations Outside the TASK-3 Pore Can Modify PKTHPP Inhibition. From the aforementioned results, it is clear that mutations in the pore modify PKTHPP inhibition of TASK-3. However, mutations in the pore may impact gating as well, and gating may have significant effects on protein conformation. For this reason, we studied the effect of mutations at residue 159 outside the pore. The M159W mutation activates TASK-3 function, as does NEM modification of M159C (Conway and Cotten, 2012). We hypothesized that gating changes via residue 159 may modify PKTHPP potency through alterations in pore accessibility and/or pore affinity. The PKTHPP IC_{50} for M159W TASK-3, relative to wild-type TASK-3, was increased approximately 4-fold from 10 nM (9–11) to 46 nM [40–52 (95% confidence), $P < 0.0001$, $n = 3$]. Similarly,

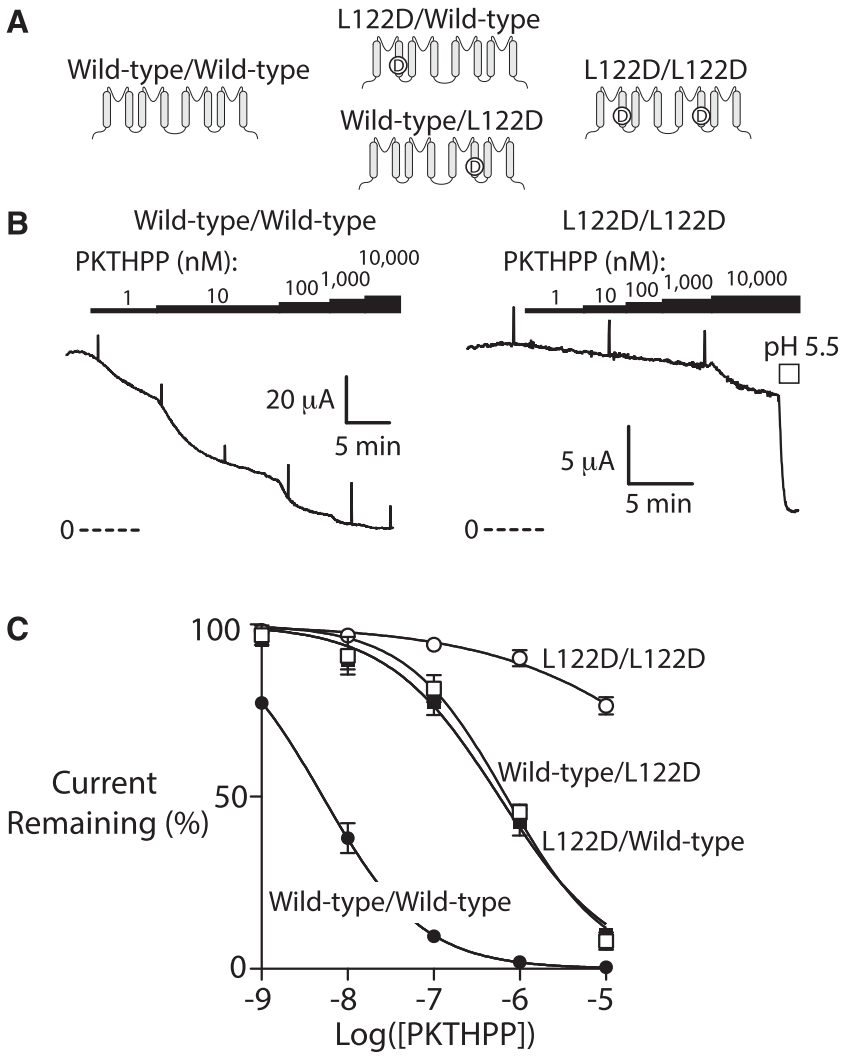

Fig. 5. A single Asp-122 in the pore is sufficient to disrupt PKTHPP inhibition of TASK-3. (A) Illustration of the location of the mutation(s) in the various TASK-3 dimer constructs. (B) Ussing chamber potassium current records using Fischer rat thyroid cell monolayers transiently expressing rat TASK-3 dimer channels (wild type/wild type or L122D/L122D). (C) Ussing chamber concentration response for PKTHPP. PKTHPP IC_{50} (in nM; data are the mean with 95% confidence interval): 5 (23–56) for wild type/wild type, 576 (431–770) for L122D/wild type***, 695 (492–981) for wild type/L122D***, and >10,000 for L122D/L122D. Data are fitted as in Fig. 3; n = at least 3 for each. ***$P < 0.001$ relative to wild-type TASK-3.

NEM modification of Cys-159, which increased the TASK-3 current 229 ± 12% ($n = 3$), caused an approximately 3-fold shift in PKTHPP IC_{50} from 10 nM (9–12) to 28 nM (23–34, $P < 0.0001$). Although significant, the shifts in PKTHPP IC_{50} were small relative to those observed with the pore mutations.

Discussion

Molecular docking and scanning site-directed aspartate mutagenesis experiments were conducted to determine the inhibitory site of action of three breathing stimulant compounds (PKTHPP, A1899, and doxapram) on TASK-3. Docking studies with a TASK-3 homology model led us to hypothesize PKTHPP and A1899 binding in the channel pore, and we undertook aspartate scanning mutagenesis studies of TASK-3 to test this pore-binding hypothesis. Of the 24 functional TASK-3 pore aspartate mutants studied, 16 displayed decreased and 5 displayed increased PKTHPP inhibitory potency. Four TASK-3 residues stood out: Leu-122, Gly-236, Leu-239, and Val-242. When mutated to aspartate (L122D, G236D, L239D, and V242D), these residues caused significant decreases in potency for PKTHPP (~100- to >1000-fold), A1899 (~50- to >1000-fold), and doxapram (~10- to 100-fold). As a point of reference, loss or gain of a strong, charged hydrogen bond (~5.45 kcal/mol) can shift ligand potency ~25,000-fold. Leu-122, Gly-236, and Leu-239 project into the TASK-3 homology model pore, and Leu-122 and Leu-239 from apposing subunits appear to interact near the transmembrane domain fenestration (Fig. 1B) and create a hydrophobic narrowing of the TASK-3 pore (Fig. 1C).

Do PKTHPP, A1899, and Doxapram Bind in the Pore? The simplest interpretation of our results is that PKTHPP, A1899, and doxapram bind in the TASK-3 pore close to residues 122, 236, and 239. Mutagenesis of these residues may lead to loss of favorable or gain of unfavorable interaction(s). Notably, every residue 122 mutation studied, including the conservative L122I substitution, diminished PKTHPP potency (Fig. 4). This implies a lack of tolerance for small structural changes and close contact between PKTHPP and residue 122. Mutations at residues 244–248 impact PKTHPP potency, but their relationships to the pore are less clear as they were not included in our homology model due to poor alignment between TASK-3 and TWIK-1 in this region.

It is interesting that three different compounds bind with high affinity in the TASK-3 pore, and that the same set of mutations, L122D, G236D, L239D, and V242D, impact each. However, the channel pore is an accessible hydrophobic cavity

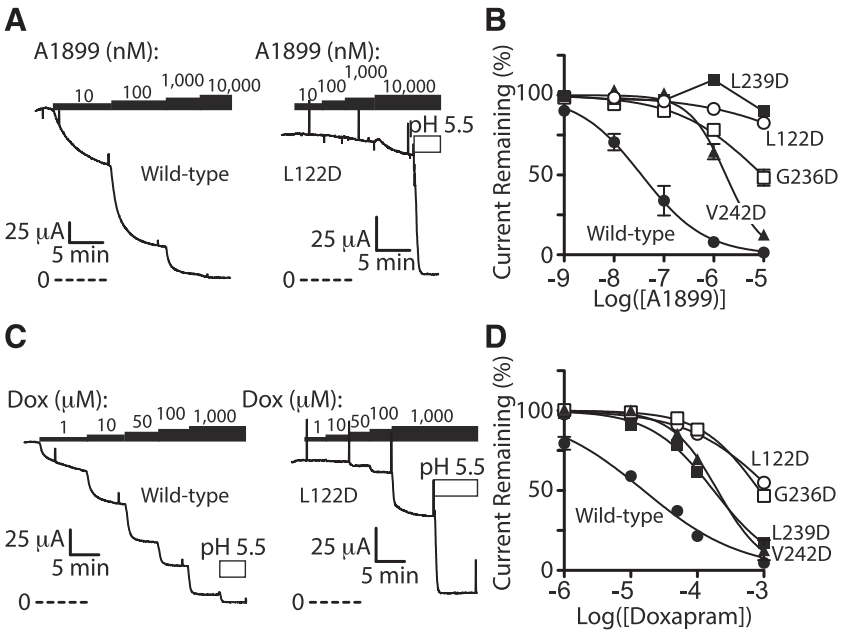

Fig. 6. L122D, G236D, L239D, and V242D mutations in the TASK-3 pore disrupt inhibition by A1899 and doxapram (Dox). (A and C) Ussing chamber potassium current records using Fischer rat thyroid cell monolayers transiently expressing rat TASK-3 channels (wild type and L122D). (B and D) Ussing chamber concentration response for A1899 and doxapram. A1899 IC_{50} (in nM; data are the mean with 95% confidence interval): 36 (23–56) for wild type, 1744 (1392–2185) for V242D***, 9490 (6432–14,000) for G236D***, >10,000 for L239D, and >10,000 for L122D. Doxapram IC_{50} (in μM): 16 (12–21) for wild type, 176 (154–201) for L239D***, 202 (163–249) for V242D***, 865 (742–1009) for G236D***, and 1349 (1096–1660) for L122D***. Data are fitted as in Fig. 3; n = at least 3 for each. ***$P < 0.001$ relative to wild-type TASK-3.

(Fig. 1C) in which a hydrophobic drug can dock. Doxapram, the least potent, is also the smallest and the least hydrophobic (Fig. 2A). Additionally, there is precedence as the hERG potassium channel binds a variety of drugs in its pore (Perry et al., 2010), and mutagenesis and docking studies suggest the pore of TASK-1 may bind a range of structurally different blocking compounds (Streit et al., 2011; Kiper et al., 2015).

Several of the mutations caused small increases in PKTHPP potency (Fig. 3). We speculate this may be due in part to a favorable interaction (e.g., a hydrogen bond) between the introduced carboxylate and the carbonyl oxygen of PKTHPP (Fig. 2A), although other effects are possible (see following section).

Mutations May Have Effects beyond Direct Binding. Mutations may modify potency through effects on binding site availability (i.e., gating and/or pore access) and/or through allosteric effects on the binding site. This applies to all mutations, including those of residues that do line the pore and those that do not. Several residues with PKTHPP potency effects direct side chains away from the pore (Ser-127, Ala-237, Val-230, Asn-240, Leu-241, and Val-242) (Fig. 2). We speculate these mutations modify pore access through a gating or pore access effect. Asn-240 and Leu-241 may reside near Met-159, which has a role in TASK-3 anesthetic activation and gating (Conway and Cotten, 2012; Bertaccini et al., 2014). Mutations at residue 159 outside the pore have small but significant effects on PKTHPP IC_{50}.

In TREK-1 and TWIK-1 tandem pore potassium channels, the gate which regulates potassium flow resides deep in the pore (Piechotta et al., 2011; Aryal et al., 2014). A hydrophobic "cuff" in the TWIK-1 pore created by Leu-146, Leu-261, and Leu-264 composes this gate. Leu-122, Gly-236, and Leu-239 of TASK-3 align with those of TWIK-1 and create a similar hydrophobic cuff in the TASK-3 pore (Figs. 1C and 7). Molecular dynamic and mutagenesis studies suggest increased polarity in the pore of TWIK-1 at residues 146 or 261 may increase pore hydration or "wetting" and overall potassium channel activity. Therefore, Leu-122, Gly-236, Leu-239, and adjacent residues of TASK-3, when mutated to aspartate, may 1) present a hydrophilic (lipid-repelling) barrier in the pore to impede inhibitor access to the hydrophobic residues deep in the pore, 2) impair drug binding by increasing water and potassium occupancy of the pore, and 3) serve as a fulcrum point for channel gating and thereby modify inhibitor binding site(s) access. These considerations are not mutually exclusive with a role in direct binding.

Agreement with Prior Studies. Streit et al. (2011) undertook a scanning alanine mutagenesis approach in the TASK-1 pore to identify residues involved in A1899 binding.

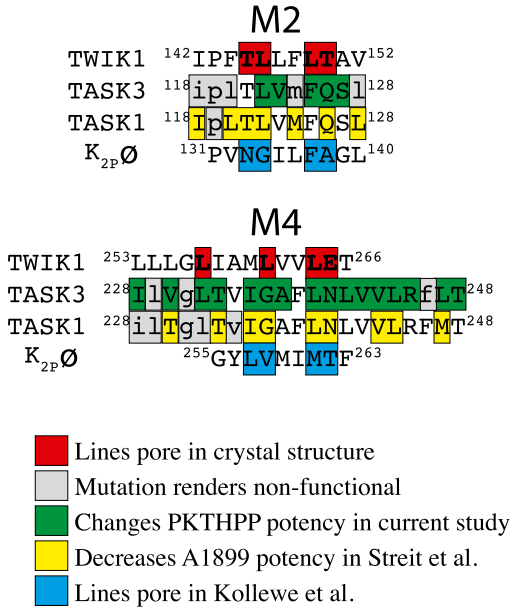

Fig. 7. Amino acid sequence alignment of TWIK-1, TASK-3, TASK-1, and $K_{2p\text{ø}}$ tandem pore potassium channels in relevant portions of M2 and M4 transmembrane domains. Data and alignment based on results published in Kollewe et al. (2009), Streit et al. (2011), and Miller and Long (2012).

Although we focused on a different compound, PKTHPP, there were similarities in our results. Of note, TASK-1 and TASK-3 sequences are nearly identical in the pore. Excluding Ile-118 and Thr-121, every residue in TASK-1 indentified by Streit et al. (2011) as contributing to A1899 binding also contributes to PKTHPP binding in TASK-3 (Figs. 3 and 7). This includes Leu-122, Gly-236, and Leu-239. The outliers, I118D, M124D, and L128D, were nonfunctional in TASK-3, and the TASK-1 mutant T121A had a minimal effect on A1899 blockade. Our results agree with those of Kollewe et al. (2009) as well. They used a compensatory countercharge approach to identify pore-lining residues in the *Drosophila* $K_{2p}ø$ tandem pore channel. Seven of the eight residues in $K_{2p}ø$ that line the pore align with residues in TASK-3 that alter PKTHPP binding (Fig. 7).

We had previously determined that doxapram is a potent inhibitor of TASK-1 and TASK-3 channels; however, TASK-1 is (~90-fold) more sensitive. Yet, doxapram sensitivity can be mostly swapped between TASK-1 and TASK-3 by swapping intracellular, carboxy-terminal domains (distal to amino acid 246) (Cotten et al., 2006). In the GIRK2 potassium channel crystal structure, the carboxy-terminal domain provides an additional gate to regulate channel pore access (Whorton and MacKinnon, 2011). We speculate, therefore, that the carboxy-terminal domains of TASK-1 and TASK-3, which share little homology, may also regulate pore access to doxapram. It will be interesting to determine if PKTHPP and A1899 potency, like doxapram, is modified by the carboxy terminus.

Implications for TASK-3 Structure and Function. Since unpaired, charged residues are unstable when buried in a hydrophobic environment, scanning aspartate mutagenesis has been used to identify water-exposed residues (Collins et al., 1997; Perutz, 1978). This assumes, of course, the pKa of the aspartate is acidic (pKa ~3.9). Though the non-functional aspartate mutants in our study could be defective for many reasons, the homology model shows most to project away from the pore into other membrane-associated helices or the membrane itself (e.g., residues 119, 120, 124, 128, and 231) (Fig. 2C). Conversely, for functional mutants, the residues mutated in general project into the pore vestibule or into the intracellular surface of the protein (Fig. 2C). The M4 domain from residue 231 to 248, excluding Phe-246, is tolerant to aspartate scanning mutagenesis implying this helix projects into an aqueous environment; Asn-240 and Leu-241, which project away from the pore (Fig. 2C), may contribute to a solvent accessible anesthetic binding vestibule (Bertaccini et al., 2014).

Leu-122 of TASK-3, which provided the strongest effects on PKTHPP potency when mutated, projects into the pore in the homology model (Fig. 1 and 2C). Consistent with this, L122E and L122D mutants provided robust currents, which contrast with the small currents provided by L122K (Fig. 4F). The positively charged lysine residue likely interferes electrostatically with conducting potassium ions. Similarly, the Birk-Barel mutation (G236R) is believed to project a positive charge into the TASK-3 pore (Barel et al., 2008). In our model, Gly-236 lines the TASK-3 pore, and the G236D mutation provides strong potassium currents and strongly shifts PKTHPP, A1899, and doxapram potency.

The properties of the TASK-3 inhibitors inform on the dimensions and properties of the TASK-3 pore. Our data suggest the TASK-3 pore is able to accommodate hydrophobic inhibitors with cLogPs of 4.2, 5.2, and 3.7 and volumes of 445, 447, and 372 $Å^3$ for PKTHPP, A1899, and doxapram, respectively. In addition to the hydrophobic narrowing caused by Leu-122 and Leu-239, the homology model suggests the TASK-3 pore is hydrophobic, which might explain its proclivity for hydrophobic blockers (Fig. 1C).

Pharmacologic targeting of TASK channels may have utility in treating a range of medical disorders including those of breathing, sleep, neoplasia, mood, and cardiac rhythm. In this study, we identified several mutations in the TASK-3 pore which modify potency of three breathing stimulants compounds, PKTHPP, A1899, and doxapram, suggesting they share a common binding site. A detailed understanding of how inhibitors interact with TASK-3 will facilitate optimization for improved selectivity, formulation, and pharmacokinetics and may guide development of inhibitors for other potassium channels. The inhibitor-resistant TASK-3 mutants may have utility when expressed in vivo (i.e., in a transgenic animal) to understand the role of TASK channel modulation in eliciting physiologic responses such as breathing stimulation.

Acknowledgments

The authors thank their laboratory colleagues Drs. Hua-Jun Feng, Stuart Forman, Youssef Jounaidi, Keith Miller, and Douglas Raines for many helpful discussion.

Authorship Contributions

Participated in research design: Chokshi, Larsen, and Cotten.
Conducted experiments: Chokshi and Larsen.
Contributed new reagents or analytic tools: Larsen, Bhayana.
Performed data analysis: Larsen, Cotten.
Wrote or contributed to the writing of the manuscript: Chokshi, Larsen, Bhayana, and Cotten.

References

Aryal P, Abd-Wahab F, Bucci G, Sansom MS, and Tucker SJ (2014) A hydrophobic barrier deep within the inner pore of the TWIK-1 K2P potassium channel. *Nat Commun* **5**:4377.

Barel O, Shalev SA, Ofir R, Cohen A, Zlotogora J, Shorer Z, Mazor G, Finer G, Khateeb S, and Zilberberg N et al. (2008) Maternally inherited Birk Barel mental retardation dysmorphism syndrome caused by a mutation in the genomically imprinted potassium channel KCNK9. *Am J Hum Genet* **83**:193–199.

Benkert P, Kunzli M, and Schwede T (2009) QMEAN server for protein model quality estimation. *Nucleic Acids Res* **37**:W510–W514.

Bertaccini EJ, Dickinson R, Trudell JR, and Franks NP (2014) Molecular modeling of a tandem two pore domain potassium channel reveals a putative binding site for general anesthetics. *ACS Chem Neurosci* **5**:1246–1252.

Brendel J, Goegelein H, Wirth K, and Kamm W (2009) inventors, Sanofi-Aventis Deutschland Gmbh, assignee. Inhibitors of the TASK-1 and TASK-3 ion channel. U.S. patent US20090149496 A1.

Brohawn SG, del Mármol J, and MacKinnon R (2012) Crystal structure of the human K2P TRAAK, a lipid- and mechano-sensitive K+ ion channel. *Science* **335**:436–441.

Buckler KJ, Williams BA, and Honore E (2000) An oxygen-, acid- and anaesthetic-sensitive TASK-like background potassium channel in rat arterial chemoreceptor cells. *J Physiol* **525**:135–142.

Callahan R, Labunskiy DA, Logvinova A, Abdallah M, Liu C, Cotten JF, and Yost CS (2004) Immunolocalization of TASK-3 (KCNK9) to a subset of cortical neurons in the rat CNS. *Biochem Biophys Res Commun* **319**:525–530.

Coburn CA, Luo Y, Cui M, Wang J, Soll R, Dong J, Hu B, Lyon MA, Santarelli VP, and Kraus RL et al. (2012) Discovery of a pharmacologically active antagonist of the two-pore-domain potassium channel K2P9.1 (TASK-3). *ChemMedChem* **7**: 123–133.

Collins A, Chuang H, Jan YN, and Jan LY (1997) Scanning mutagenesis of the putative transmembrane segments of Kir2.1, an inward rectifier potassium channel. *Proc Natl Acad Sci USA* **94**:5456–5460.

Conway KE and Cotten JF (2012) Covalent modification of a volatile anesthetic regulatory site activates TASK-3 (KCNK9) tandem-pore potassium channels. *Mol Pharmacol* **81**:393–400.

Cotten JF (2013) TASK-1 (KCNK3) and TASK-3 (KCNK9) tandem pore potassium channel antagonists stimulate breathing in isoflurane-anesthetized rats. *Anesth Analg* **116**:810–816.

Cotten JF, Keshavaprasad B, Laster MJ, Eger EI, 2nd, and Yost CS (2006) The ventilatory stimulant doxapram inhibits TASK tandem pore (K2P) potassium channel function but does not affect minimum alveolar anesthetic concentration. *Anesth Analg* **102**:779–785.

Czirják G and Enyedi P (2002) TASK-3 dominates the background potassium conductance in rat adrenal glomerulosa cells. *Mol Endocrinol* **16**:621–629.
Davies LA, Hu C, Guagliardo NA, Sen N, Chen X, Talley EM, Carey RM, Bayliss DA, and Barrett PQ (2008) TASK channel deletion in mice causes primary hyperaldosteronism. *Proc Natl Acad Sci USA* **105**:2203–2208.
Decher N, Wemhöner K, Rinné S, Netter MF, Zuzarte M, Aller MI, Kaufmann SG, Li XT, Meuth SG, and Daut J et al. (2011) Knock-out of the potassium channel TASK-1 leads to a prolonged QT interval and a disturbed QRS complex. *Cell Physiol Biochem* **28**:77–86.
Dong YY, Pike AC, Mackenzie A, McClenaghan C, Aryal P, Dong L, Quigley A, Grieben M, Goubin S, and Mukhopadhyay S et al. (2015) K2P channel gating mechanisms revealed by structures of TREK-2 and a complex with Prozac. *Science* **347**:1256–1259.
Donner BC, Schullenberg M, Geduldig N, Hüning A, Mersmann J, Zacharowski K, Kovacevic A, Decking U, Aller MI, and Schmidt KG (2011) Functional role of TASK-1 in the heart: studies in TASK-1-deficient mice show prolonged cardiac repolarization and reduced heart rate variability. *Basic Res Cardiol* **106**:75–87.
Flaherty DP, Simpson DS, Miller M, Maki BE, Zou B, Shi J, Wu M, McManus OB, Aubé J, and Li M et al. (2014) Potent and selective inhibitors of the TASK-1 potassium channel through chemical optimization of a bis-amide scaffold. *Bioorg Med Chem Lett* **24**:3968–3973.
Gierten J, Ficker E, Bloehs R, Schweizer PA, Zitron E, Scholz E, Karle C, Katus HA, and Thomas D (2010) The human cardiac K2P3.1 (TASK-1) potassium leak channel is a molecular target for the class III antiarrhythmic drug amiodarone. *Naunyn Schmiedebergs Arch Pharmacol* **381**:261–270.
Gotter AL, Santarelli VP, Doran SM, Tannenbaum PL, Kraus RL, Rosahl TW, Meziane H, Montial M, Reiss DR, and Wessner K et al. (2011) TASK-3 as a potential antidepressant target. *Brain Res* **1416**:69–79.
Guagliardo NA, Yao J, Hu C, Schertz EM, Tyson DA, Carey RM, Bayliss DA, and Barrett PQ (2012) TASK-3 channel deletion in mice recapitulates low-renin essential hypertension. *Hypertension* **59**:999–1005.
Kim D, Cavanaugh EJ, Kim I, and Carroll JL (2009) Heteromeric TASK-1/TASK-3 is the major oxygen-sensitive background K+ channel in rat carotid body glomus cells. *J Physiol* **587**:2963–2975.
Kindler CH, Yost CS, and Gray AT (1999) Local anesthetic inhibition of baseline potassium channels with two pore domains in tandem. *Anesthesiology* **90**: 1092–1102.
Kiper AK, Rinné S, Rolfes C, Ramírez D, Seebohm G, Netter MF, González W, and Decher N (2015) Kv1.5 blockers preferentially inhibit TASK-1 channels: TASK-1 as a target against atrial fibrillation and obstructive sleep apnea? *Pflugers Arch* **467**:1081–1090.
Koizumi H, Smerin SE, Yamanishi T, Moorjani BR, Zhang R, and Smith JC (2010) TASK channels contribute to the K+-dominated leak current regulating respiratory rhythm generation in vitro. *J Neurosci* **30**:4273–4284.
Kollewe A, Lau AY, Sullivan A, Roux B, and Goldstein SA (2009) A structural model for K2P potassium channels based on 23 pairs of interacting sites and continuum electrostatics. *J Gen Physiol* **134**:53–68.
Lazarenko RM, Willcox SC, Shu S, Berg AP, Jevtovic-Todorovic V, Talley EM, Chen X, and Bayliss DA (2010) Motoneuronal TASK channels contribute to immobilizing effects of inhalational general anesthetics. *J Neurosci* **30**:7691–7704.
Liang B, Soka M, Christensen AH, Olesen MS, Larsen AP, Knop FK, Wang F, Nielsen JB, Andersen MN, and Humphreys D et al. (2014) Genetic variation in the two-pore domain potassium channel, TASK-1, may contribute to an atrial substrate for arrhythmogenesis. *J Mol Cell Cardiol* **67**:69–76.
Limberg SH, Netter MF, Rolfes C, Rinné S, Schlichthörl G, Zuzarte M, Vassiliou T, Moosdorf R, Wulf H, and Daut J et al. (2011) TASK-1 channels may modulate action potential duration of human atrial cardiomyocytes. *Cell Physiol Biochem* **28**:613–624.
Lolicato M, Riegelhaupt PM, Arrigoni C, Clark KA, and Minor DL, Jr (2014) Transmembrane helix straightening and buckling underlies activation of mechanosensitive and thermosensitive K(2P) channels. *Neuron* **84**:1198–1212.
Lunsford CD, Cale AD, Jr, Ward JW, Franko BV, and Jenkins H (1964) 4-(Beta-Substituted Ethyl)-3,3-Diphenyl-2-Pyrrolidinones. A New Series of Cns Stimulants. *J Med Chem* **7**:302–310.
Ma L, Roman-Campos D, Austin ED, Eyries M, Sampson KS, Soubrier F, Germain M, Trégouët DA, Borczuk A, and Rosenzweig EB et al. (2013) A novel channelopathy in pulmonary arterial hypertension. *N Engl J Med* **369**:351–361.
Miller AN and Long SB (2012) Crystal structure of the human two-pore domain potassium channel K2P1. *Science* **335**:432–436.
Moitessier N, Henry C, Maigret B, and Chapleur Y (2004) Combining pharmacophore search, automated docking, and molecular dynamics simulations as a novel strategy for flexible docking. Proof of concept: docking of arginine-glycine-aspartic acid-like compounds into the alphavbeta3 binding site. *J Med Chem* **47**: 4178–4187.
Mu D, Chen L, Zhang X, See LH, Koch CM, Yen C, Tong JJ, Spiegel L, Nguyen KC, and Servoss A et al. (2003) Genomic amplification and oncogenic properties of the KCNK9 potassium channel gene. *Cancer Cell* **3**:297–302.
Mulkey DK, Talley EM, Stornetta RL, Siegel AR, West GH, Chen X, Sen N, Mistry AM, Guyenet PG, and Bayliss DA (2007) TASK channels determine pH sensitivity in select respiratory neurons but do not contribute to central respiratory chemosensitivity. *J Neurosci* **27**:14049–14058.
Olschewski A, Li Y, Tang B, Hanze J, Eul B, Bohle RM, Wilhelm J, Morty RE, Brau ME, and Weir EK et al. (2006) Impact of TASK-1 in human pulmonary artery smooth muscle cells. *Circ Res* **98**:1072–1080.
Ortega-Saenz P, Levitsky KL, Marcos-Almaraz MT, Bonilla-Henao V, Pascual A, and Lopez-Barneo J (2010) Carotid body chemosensory responses in mice deficient of TASK channels. *J Gen Physiol* **135**(4):379–392.
Pang DS, Robledo CJ, Carr DR, Gent TC, Vyssotski AL, Caley A, Zecharia AY, Wisden W, Brickley SG, and Franks NP (2009) An unexpected role for TASK-3 potassium channels in network oscillations with implications for sleep mechanisms and anesthetic action. *Proc Natl Acad Sci USA* **106**:17546–17551.
Perry M, Sanguinetti M, and Mitcheson J (2010) Revealing the structural basis of action of hERG potassium channel activators and blockers. *J Physiol* **588**: 3157–3167.
Perutz MF (1978) Electrostatic effects in proteins. *Science* **201**:1187–1191.
Petric S, Clasen L, van Wessel C, Geduldig N, Ding Z, Schullenberg M, Mersmann J, Zacharowski K, Aller MI, and Schmidt KG et al. (2012) In vivo electrophysiological characterization of TASK-1 deficient mice. *Cell Physiol Biochem* **30**: 523–537.
Pettersen EF, Goddard TD, Huang CC, Couch GS, Greenblatt DM, Meng EC, and Ferrin TE (2004) UCSF Chimera–a visualization system for exploratory research and analysis. *J Comput Chem* **25**:1605–1612.
Peukert S, Brendel J, Pirard B, Brüggemann A, Below P, Kleemann HW, Hemmerle H, and Schmidt W (2003) Identification, synthesis, and activity of novel blockers of the voltage-gated potassium channel Kv1.5. *J Med Chem* **46**:486–498.
Piechotta PL, Rapedius M, Stansfeld PJ, Bollepalli MK, Ehrlich G, Andres-Enguix I, Fritzenschaft H, Decher N, Sansom MS, and Tucker SJ et al. (2011) The pore structure and gating mechanism of K2P channels. *EMBO J* **30**:3607–3619.
Putzke C, Wemhöner K, Sachse FB, Rinné S, Schlichthörl G, Li XT, Jaé L, Eckhardt I, Wischmeyer E, and Wulf H et al. (2007) The acid-sensitive potassium channel TASK-1 in rat cardiac muscle. *Cardiovasc Res* **75**:59–68.
Schmidt C, Wiedmann F, Langer C, Tristram F, Anand P, Wenzel W, Lugenbiel P, Schweizer PA, Katus HA, and Thomas D (2014) Cloning, functional characterization, and remodeling of K2P3.1 (TASK-1) potassium channels in a porcine model of atrial fibrillation and heart failure. *Heart Rhythm* **11**:1798–1805.
Staudacher K, Staudacher I, Ficker E, Seyler C, Gierten J, Kisselbach J, Rahm AK, Trappe K, Schweizer PA, and Becker R et al. (2011) Carvedilol targets human K2P 3.1 (TASK1) K+ leak channels. *Br J Pharmacol* **163**:1099–1110.
Sheppard DN, Carson MR, Ostedgaard LS, Denning GM, and Welsh MJ (1994) Expression of cystic fibrosis transmembrane conductance regulator in a model epithelium. *Am J Physiol* **266**(4 Pt 1):L405–413.
Streit AK, Netter MF, Kempf F, Walecki M, Rinné S, Bollepalli MK, Preisig-Müller R, Renigunta V, Daut J, and Baukrowitz T et al. (2011) A specific two-pore domain potassium channel blocker defines the structure of the TASK-1 open pore. *J Biol Chem* **286**:13977–13984.
Whorton MR and MacKinnon R (2011) Crystal structure of the mammalian GIRK2 K+ channel and gating regulation by G proteins, PIP2, and sodium. *Cell* **147**: 199–208.
Wirth KJ, Brendel J, Steinmeyer K, Linz DK, Rütten H, and Gögelein H (2007) In vitro and in vivo effects of the atrial selective antiarrhythmic compound AVE1231. *J Cardiovasc Pharmacol* **49**:197–206.
Wirth KJ, Paehler T, Rosenstein B, Knobloch K, Maier T, Frenzel J, J, Busch AE, and Bleich M (2003) Atrial effects of the novel K(+)-channel-blocker AVE0118 in anesthetized pigs. *Cardiovasc Res* **60**:298–306.
Wirth KJ, Steinmeyer K, and Ruetten H (2013) Sensitization of upper airway mechanoreceptors as a new pharmacologic principle to treat obstructive sleep apnea: investigations with AVE0118 in anesthetized pigs. *Sleep* **36**:699–708.
Yost CS (2003) Update on tandem pore (2P) domain K+ channels. *Curr Drug Targets* **4**:347–351.

Address correspondence to: Dr. Joseph F. Cotten, Massachusetts General Hospital, Department of Anesthesia, Critical Care, and Pain Medicine, 55 Fruit Street, GRB 444, Boston, MA 02114. E-mail: jcotten@mgh.harvard.edu